Avalanches in vanadium sesquioxide nanodevices

Siming Wang, Juan Gabriel Ramírez, and Ivan K. Schuller

Phys. Rev. B **92**, 085150 — Published 28 August 2015

DOI: 10.1103/PhysRevB.92.085150

Avalanches in Vanadium Sesquioxide Nanodevices

Siming Wang[1,2,3,]*, Juan Gabriel Ramírez[1,4], and Ivan K. Schuller[1,2]

[1]*Department of Physics and Center for Advanced Nanoscience, University of California, San Diego, La Jolla, California 92093, USA*

[2]*Materials Science and Engineering Program, University of California, San Diego, La Jolla, California 92093, USA*

[3]*Materials Science Division, Lawrence Berkeley National Laboratory, Berkeley, California 94720, USA*

[4]*Department of Physics, Universidad de los Andes, Bogotá 111711, Colombia*

The resistance versus temperature across the metal insulator transition (MIT) of V_2O_3 nanodevices exhibits multiple discontinuous jumps. The jump sizes range over 3 orders of magnitude in resistance and their distribution follows a power law, implying that the MIT of V_2O_3 occurs through avalanches. While the maximum jump size depends on the device size, the power law exponent for V_2O_3 is independent of device geometry and different than the one found earlier in VO_2. A two dimensional random percolation model exhibits a power law distribution different from the one found in V_2O_3. Instead, the model gives a similar exponent found in another vanadium oxide, VO_2. Our results suggest that the MITs of VO_2 and V_2O_3 are produced by different mechanisms.

The physical properties of a condensed matter system (crystal structure, resistance, magnetization, strain, etc.) can vary discontinuously when driven by external forces such as temperature [1-3], magnetic field [4-9], stress [10], and chemical potential [11]. The size of these changes can range over many orders of magnitude. This phenomenon has been referred as crackling noise or avalanches [12,13]. Avalanches can be observed in a variety of materials, including Barkhausen noise in ferromagnets [4-6], field-driven transformation of phase-separated manganites [7], Martensitic transformations [1], microfractures [10], vortex motion in type-II superconductors [8,9], hydrogen precipitation in niobium [2], and helium condensation in porous materials [11]. The distribution of the avalanche sizes follows a power law, $N \propto A^{-\alpha}$, where N is the number of the avalanches, A is the size of the avalanches and α is the power law exponent. The existence of a power law indicates the absence of characteristic length scales in these systems, i.e. the systems are self-similar at all length scales [12,13]. Recently, multiple avalanches were observed across the first-order metal-insulator transition (MIT) of VO_2 as jumps in the resistance vs. temperature (R-T) measurements [3]. When metallic and insulating phases coexist [14-16] in VO_2, temperature induced resistance jumps ranging over 2 – 3 orders of magnitude appear. These jumps follow a power law distribution [3]. Furthermore, the power law exponent is independent of device geometry or temperature sweep rate, indicating that the exponent is an intrinsic property of VO_2 [3]. A theoretical model has been proposed to explain the avalanches in VO_2 with a two dimensional (2D) random percolation model [17].

Similar to VO_2, other materials undergoing inhomogeneous first-order MITs are expected to exhibit avalanches. For instance, V_2O_3, another member of the vanadium oxide family, undergoes a first-order MIT at 165K [18]. The MITs in VO_2 and V_2O_3 are phenomenologically similar, i.e. the resistivity of the materials changes by several decades at a stoichiometry-

dependent transition temperature, accompanied by a first order structural phase transition. However, a recent study of ion irradiation damage have shown that the mechanisms of the MITs in VO_2 and V_2O_3 are different [19]. This study is performed on macroscopic thin films but the microscopic difference between the two materials has not been yet explored.

In this Rapid Communication, we report avalanches in the MIT of V_2O_3. Temperature-driven avalanches are observed in R-T measurements of V_2O_3 nanodevices with resistance jumps ranging over 3 – 4 orders of magnitude. The largest jumps depend on the device dimensions, while the resistance jump sizes follow a power law distribution, with a power law exponent independent of device geometry. Furthermore, the avalanches of V_2O_3 and VO_2 are compared with a numerical model based on 2D random percolation. VO_2 and V_2O_3 exhibit different power law exponents, suggesting that the MITs in these two materials may occur through different mechanisms. Our observations highlight the microscopic difference between two inhomogeneous materials, which are otherwise similar at the macroscopic scale.

The deposition conditions of the V_2O_3 thin films were described in Ref. [20]. The film thickness is fixed to 100 nm in this study. Single crystalline growth of the films is established from X-ray diffraction [19,21,22]. All the devices are fabricated on two V_2O_3 thin films deposited in two consecutive depositions using sapphire substrates from the same wafer. This ensures that the structure and resistivity of V_2O_3 are identical. V_2O_3 devices were fabricated with standard e-beam lithography and lift-off process. For the metallic electrodes, a 10 nm vanadium layer was deposited as an adhesion layer followed by a 50 nm gold layer for electrical contact. The device length is the distance between two metallic electrodes and device width is given by the width of the electrodes (see FIG. 1(a)). The metallic electrodes are connected to macroscopic pads for electrical connections using standard photolithography techniques. The resistance of the

devices was measured in a 2-probe configuration with a current source and a voltmeter. The current for all the measurements is fixed to 100 nA to ensure that the electric field across the devices is on the order of 10^3 V/cm when the metal insulator transition takes place. This electric field is two orders of magnitude lower than that used to drive a voltage induced transition [23], so the current and voltage do not affect the avalanches in these measurements. For each device, 10 consecutive R-T curves were measured at a constant 1 K/min temperature sweep rate and a 5Hz sampling rate in order to assure the same sampling number for all the devices and enough resolution of the avalanche over three decades [1,24].

The main panel in Fig. 1 shows the heating branches of 5 consecutive R-T measurements of a 1 × 2 μm^2 V_2O_3 device from 145 K – 157.5 K. The full hysteresis loops are shown in Fig. 1(b). The device exhibits a 5 order magnitude MIT over 20 K with a 5 K thermal hysteresis centered at 150 K. The MIT in these nanodevices is similar to that in a V_2O_3 thin film, indicating that the lithographic processes do not modify the material. Resistance jumps of various sizes are observed from the onset to the end of the MIT. There are a few large jumps of up to 2×10^4 Ω, which account for more than 50 % of the resistance change. The rest of the jumps are smaller, ranging from a few kilo ohms to a few ohms, limited by the measurement resolution. This indicates that the MIT of V_2O_3 takes place inhomogeneously at the nanoscale, due to the coexistence of the insulating and metallic phases [25], and the MIT occurs through a series of discontinuous transitions over a broad range of magnitudes.

We define the jump size with two consecutive data points (T_1,R_1) and (T_2,R_2) from the R-T measurements ($T_1 < T_2$):

$$\Delta R/R = (R_1 - R_2)/R_1. \quad (1)$$

Note that we choose $\Delta R/R$ instead of $\Delta R = R_1 - R_2$ to measure the jump size. The instrumental noise (about 0.1 %) can give rise to 100's or 1000's of Ohms fluctuation in the resistance measurements when the oxide is in the insulating phase. This introduces errors in the statistics of ΔR, which can be avoided using $\Delta R / R$ with a minimum cut-off $(\Delta R / R)_{min} = 0.002 - 0.005$.

Fig. 2 shows the maximum jump size as a function of the device length. All the devices are fabricated with the same V_2O_3 thin film and the device width is kept constant (2 μm) for all devices. Each data point in Fig. 2 is calculated by averaging the maximum jumps from the heating (red solid circles) or cooling (blue open circles) branches of the R-T for each device length (L). The error bars are obtained from the standard deviation. For both heating and cooling, the average maximum jump size decreases with the increasing device length. For each device length, the maximum jump sizes for heating and cooling are the same within error bar. Similar geometrical dependence of the largest jump was previously reported in VO_2 nanodevices [3]. A linear fit of the maximum jump size as a function of the device length intercepts the x-axis at L = 3.4 μm, indicating that the R-T curve becomes continuous for a device length above 3.4 μm. This value is on the same order of magnitude as previously reported for VO_2 devices [3].

Fig. 3 shows the histogram of the resistance jump sizes of the 1 × 2 μm^2 V_2O_3 device (black circles). The number of jumps (N) is obtained from a logarithmic binning of the resistance jumps calculated using Eq. (1). The histogram is fitted to a power law, $N \propto (\Delta R/R)^{-\alpha}$, using the maximum likelihood method [26] (red solid line in Fig. 3). The linear behavior of the histogram on a log-log scale plot shows that the jump size distribution follows a power law, which is a main signature of avalanches [12,13]. The power law exponent of this device is $\alpha = 2.22 \pm 0.03$. We chose the minimum cut-off $(\Delta R/R)_{min} = 0.002 - 0.005$ in the maximum likelihood fit. Within this range, the power law exponent α does not change when $(\Delta R/R)_{min}$ is varied. Fig. 4(b) further

shows the geometrical dependence of the power law exponent with the device length (red solid and open circles). The exponents vary between 2.1 and 2.7 for all the devices. As opposed to the maximum jump size, we did not observe a correlation between the exponents and the device length for either heating or cooling. This suggests that the power law exponent of the V_2O_3 device is independent of device geometry. In a separate sample, we vary the device width from 1 – 5 μm while keeping the device length at 500 nm. The exponents vary in the same range and show no geometrical dependence either. We found a normal distribution of the exponents for all the devices in both samples with a mean value of 2.36, indicated by the red dash line in Fig. 4(b) [27].

It is important to note that the resistance jumps ΔR are not directly related to the volume fraction of the insulating and metallic phases during the MIT, but are connected to the percolation across the electrodes [3,28]. Therefore, ΔR does not reflect directly the role of an avalanche in the percolation. A large ΔR plays no significant role in the percolation if the temperature is low (below 140 K) and the resistance of the device is high. On the other hand, ΔR/R reflects the percolation more faithfully than ΔR. The V_2O_3 MIT takes place through metallic domain formation at the nanoscale [25]. Each domain switching causes a resistance jump [3,29]. The largest jump occurs when the two electrodes are connected by a metallic path, i.e. the system reaches its percolation threshold [28]. As the device length decreases, fewer metallic domains are required to form a metallic path to reach percolation. As a result, one domain switching induces a larger jump. This explains the geometrical dependence of the device length shown in Fig. 2. On the other hand, the power law distribution of the jump sizes does not depend on the device dimension, implying that the power law is an intrinsic property of V_2O_3.

To understand the origin of the power law distribution of jump sizes, we performed numerical simulations with a random percolation model [3,17]. The V_2O_3 device is simulated with a 2D square lattice [3]. Each lattice site in the model represents a 50×50 nm^2 V_2O_3 domain. We assumed that the MIT within a 50×50 nm^2 V_2O_3 domain takes place independently from its neighbors. The transition temperature of the domains follows a Gaussian distribution with a mean value of 153.3 K and a standard deviation of 10 K in agreement with the experimental sample inhomogeneity. With this the simulated R-T reproduce the transition temperature and width of the heating branches from the measured R-T, as shown in Fig. 4(a). When a domain switches, its resistance changes from 1.5 MΩ (insulating phase) to 150 Ω (metallic phase). The current flows in and out of the network through two gold electrodes with zero resistance at the two opposite ends of the lattice. For each temperature, the network resistance is calculated by solving the Kirchhoff equations for all the domains [28]. Note that we neglect the low temperature semiconducting temperature dependence. The insulating vanadium oxide resistance decreases exponentially with increasing temperature, but this is not reflected in the MIT avalanches. As a result, the simulated R-T curves do not exhibit the "rounded" part of the measured R-T curves shown in Fig. 4(a).

We found resistance jumps over several orders of magnitude in the simulated R-T curves, similar to the V_2O_3 devices as shown in Fig. 4(a). The maximum jump size of the simulated R-T curves are larger than in the measurements, implying that a smaller domain size should be used in the simulation. However, due to numerical limitations the domain size cannot be further reduced. The jump sizes ($\Delta R/R$) in the simulations also follow a power law distribution. Fig. 4(b) shows the geometrical dependence of the power law exponent α from the simulation (black solid squares). The power law exponents for different device lengths are all close to 2.04 and

independent of heating or cooling. This value is independent of domain size, mean value of the transition temperature, and standard deviation. This supports the previous claim that the power law exponent is an intrinsic property of the model. Thus the 2.04 power law exponent found for the percolation in a 2D square lattice is lower than that found experimentally for V_2O_3.

Fig. 4(b) further compares the power law exponent of V_2O_3 (red solid and open circles) with another vanadium oxide, VO_2 (blue solid and open triangles), which shows a similar macroscopic first order MIT [18]. The power law exponent for VO_2 [3,17] can be calculated by fitting the resistive histogram to the power law $N \propto (\Delta R/R)^{-\alpha}$, instead of $N \propto (\Delta R)^{-\alpha}$ used in Ref. [3]. The exponent $\alpha = 1.9 - 2.4$ for all the VO_2 devices, with a mean value of 2.09. This mean value for VO_2 is close to the simulated value from the 2D random percolation model, which has been used to describe the MIT in VO_2 devices [17]. However, the power law exponent for V_2O_3 is higher than for VO_2 and the simulation. We used a t-test [30] to compare the difference between the mean values of the exponents for VO_2 and V_2O_3. The test showed that the probability for the two means to be equal is only 0.07% [31].

Since the resistance jumps are measures of the percolation, different power law exponents could result from different types of percolations. This implies that a 2D random percolation model is not sufficient to describe the MIT for V_2O_3 and that the mechanisms of the MITs in VO_2 and V_2O_3 may be different. The VO_2 and V_2O_3 electronic nanostructures must be different when the insulating and metallic phases coexist during the hysteretic MIT. This implies possibly a different mechanisms involved in the MITs of the two materials.

Our statistical analysis of avalanches in different vanadium oxides reflects the differences at the nanoscale for inhomogeneous materials, which are otherwise similar at the macroscopic scale. The formation of the nanoscale metallic domains has been observed with low temperature

scanning electron microscopy when the MIT of V_2O_3 is induced by the voltage [25]. However, the MITs induced by temperature and voltage occurs through different types of percolations [17]. Scanning near-field infrared microscopy (SNIM) [14], scanning tunneling microscopy [32] or scanning tunneling spectroscopy [15] can image the electronic phase coexistence of vanadium oxides at the nanoscale during the MIT and provide further information about the percolation. Nanoscale phase coexistence of the temperature induced MIT of V_2O_3 has recently been confirmed by cryogenic s-SNOM measurements [33]. Interestingly, the phase coexistence in V_2O_3 does not correlate with the microstructure of the film, but is likely caused by the stress field during the structural phase transition [33]. Note that we showed a "cut-off" length 3.4 μm in Fig. 2 at which the R-T curves become continuous. This length scale indicates a maximum avalanche size driven by the stress, which gives rise to the physical upper limit of the avalanches. A theoretical model can be built to relate the s-SNOM images to our R-T measurements, but that is beyond the scope of the present work.

To summarize, we studied the avalanches in the MIT of V_2O_3 devices. Multiple jumps in the resistance were observed in the R-T measurements of V_2O_3 devices with different sizes at the nanoscale. The maximum jump sizes in the R-T characteristics increase with decreasing device dimensions. It indicates that the maximum jumps which depend on the device geometry are extrinsic. A power law distribution is found for the resistance jumps in the $\Delta R/R = 10^{-3}$ to 10^{-1} range. The power law exponent shows no geometrical dependence. This implies that the power law exponent is an intrinsic properties of the V_2O_3. The power law exponent of V_2O_3 was compared to VO_2 and a 2D random percolation model. While the MIT of the VO_2 devices has the same power law exponent as the 2D random percolation model, the MIT of the V_2O_3 devices shows a different power law exponent. This indicates that the MITs of VO_2 and V_2O_3 occur

through different mechanisms. Our study on the microscopic scale provides the means to discriminate the MIT mechanisms for materials which exhibit otherwise similar macroscopic properties.

Work supported by AFOSR Grant No. FA9550-12-1-0381. One of us (IKS) thanks the DoD for a NSSEFF fellowship. One of us (IKS) thanks the US Department of Defense for a National Security Science and Engineering Faculty Fellowship (NSSEFF).

* simingwang@lbl.gov

[1] E. Vives, J. Ortin, L. Manosa, I. Rafols, R. Perez-Magrane, and A. Planes, Phys. Rev. Lett. **72**, 1694 (1994).

[2] G. Cannelli, R. Cantelli, and F. Cordero, Phys. Rev. Lett. **70**, 3923 (1993).

[3] A. Sharoni, J. G. Ramírez, and I. K. Schuller, Phys. Rev. Lett. **101**, 026404 (2008).

[4] H. Barkhausen, Phys. Z. **20**, 401 (1919).

[5] H. Bittel, IEEE Trans. Magn. **5**, 359 (1969).

[6] P. J. Cote and L. V. Meisel, Phys. Rev. Lett. **67**, 1334 (1991).

[7] V. Hardy, S. Majumdar, M. R. Lees, D. McK. Paul, C. Yaicle, and M. Hervieu, Phys. Rev. B **70**, 104423 (2004).

[8] S. Field, J. Witt, F. Nori, and X. Ling, Phys. Rev. Lett. **74**, 1206 (1995).

[9] E. Altshuler, T. H. Johansen, Y. Paltiel, P. Jin, K. E. Bassler, O. Ramos, Q. Y. Chen, G. F. Reiter, E. Zeldov, and C. W. Chu, Phys. Rev. B **70**, 140505 (2004).

[10] A. Petri, G. Paparo, A. Vespignani, A. Alippi, and M. Costantini, Phys. Rev. Lett. **73**, 3423 (1994).

[11] M. P. Lilly, P. T. Finley, and R. B. Hallock, Phys. Rev. Lett. **71**, 4186 (1993).

[12] J. P. Sethna, K. A. Dahmen, and C. R. Myers, Nature **410**, 242 (2001).

[13] L. T. Donald, Rep. Prog. Phys. **62**, 1377 (1999).

[14] M. M. Qazilbash, M. Brehm, B.-G. Chae, P.-C. Ho, G. O. Andreev, B.-J. Kim, S. J. Yun, A. V. Balatsky, M. B. Maple, F. Keilmann, H.-T. Kim, and D. N. Basov, Science **318**, 1750 (2007).

[15] Y. J. Chang, J. S. Yang, Y. S. Kim, D. H. Kim, T. W. Noh, D.-W. Kim, E. Oh, B. Kahng, and J. S. Chung, Phys. Rev. B **76**, 075118 (2007).

[16] J. G. Ramírez, A. Sharoni, Y. Dubi, M. E. Gómez, and I. K. Schuller, Phys. Rev. B **79**, 235110 (2009).

[17] A. Shekhawat, S. Papanikolaou, S. Zapperi, and J. P. Sethna, Phys. Rev. Lett. 107, 276401 (2011).

[18] F. J. Morin, Phys. Rev. Lett. **3**, 34 (1959).

[19] J. G. Ramírez, T. Saerbeck, S. Wang, J. Trastoy, M. Malnou, J. Lesueur, J.-P. Crocombette, J. E. Villegas, and I. K. Schuller, Phys. Rev. B **91**, 205123 (2015).

[20] M. K. Stewart, D. Brownstead, S. Wang, K. G. West, J. G. Ramírez, M. M. Qazilbash, N. B. Perkins, I. K. Schuller, and D. N. Basov, Phys. Rev. B **85**, 205113 (2012).

[21] J. de la Venta, S. Wang, T. Saerbeck, J. G. Ramírez, I. Valmianski, and I. K. Schuller, Appl. Phys. Lett. **104**, 062410 (2014).

[22] T. Saerbeck, J. de la Venta, S. Wang, J. G. Ramírez, M. Erekhinsky, I. Valmianski, and I. K. Schuller, J. Mater. Res. **29**, 2353 (2014).

[23] H.-T. Kim, B.-G. Chae, D.-H. Youn, S.-L. Maeng, G. Kim, K.-Y. Kang, and Y.-S. Lim, New J. Phys. **6**, 52 (2004).

[24] E. Puppin, Phys. Rev. Lett. **84**, 5415 (2000).

[25] S. Guénon, S. Scharinger, S. Wang, J. G. Ramírez, D. Koelle, R. Kleiner, and I. K. Schuller, Europhys. Lett. **101**, 57003 (2013).

[26] A. Clauset, C. R. Shalizi, and M. E. J. Newman, SIAM Rev. **51**, 661 (2009).

[27] The average exponent for V_2O_3 was obtained from two samples. We varied the device length for one of the samples (4 devices in total, shown by the red symbols in FIG. 4(b)) and varied the device width for the other (5 devices in total, not shown in the figures). The average exponent was calculated from 9 devices and 18 measured exponents (heating and cooling).

[28] M. Taya, *Electronic Composites* (Cambridge University Press, New York, 2005).

[29] H.-Y. Zhai, J. X. Ma, D. T. Gillaspie, X. G. Zhang, T. Z. Ward, E. W. Plummer, and J. Shen, Phys. Rev. Lett. **97**, 167201 (2006).

[30] D. S. Moore, *The basic practice of statistics* (W. H. Freeman and Company, New York, 2007), 4th edn., p. 464 - 469.

[31] The power law exponents of V_2O_3 includes 18 experimental data points and that of VO_2 includes 10 experimental data points. The distributions of the exponents for both VO_2 and V_2O_3 follow Gaussian functions with different standard deviations. We chose the t-test model for two sample with unequal sample sizes and unequal variances. See Ref. [30] for more details.

[32] Y. Kohsaka, C. Taylor, K. Fujita, A. Schmidt, C. Lupien, T. Hanaguri, M. Azuma, M. Takano, H. Eisaki, H. Takagi, S. Uchida, and J. C. Davis, Science **315**, 1380 (2007).

[33] A. S. McLeod, E. van Heuman, J. G. Ramírez, S. Wang, T. Saerbeck, S. Guénon, M. Goldflam, L. Anderegg, P. Kelly, A. Muller, M. Liu, I. K. Schuller, and D. N. Basov, To be published.

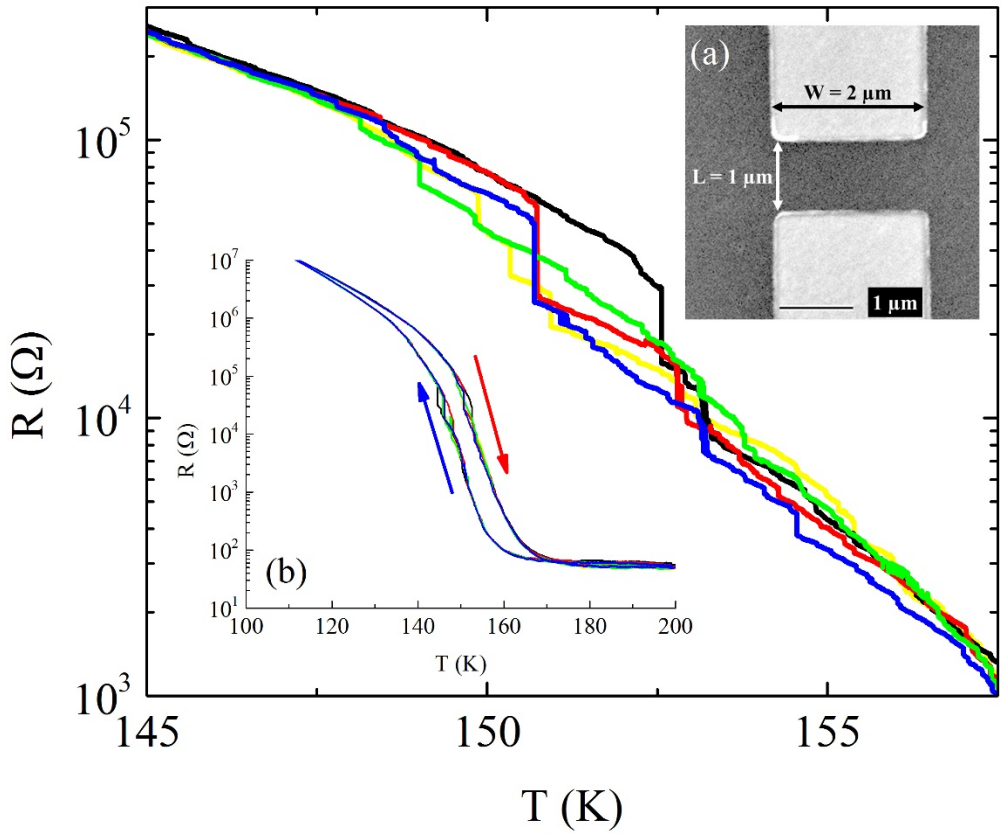

FIG. 1 (color online). The heating branches of five consecutive R-T measurements of a 1 × 2 μm^2 V_2O_3 device as indicated by different colors. The main panel shows the temperature between 145 K and 157.5 K. This range contains the largest jumps. (a) SEM image indicating the device length (L = 1 μm) and width (W = 2 μm). (b) The full hysteresis loop of the device. The red (blue) arrow indicates the heating (cooling) branches.

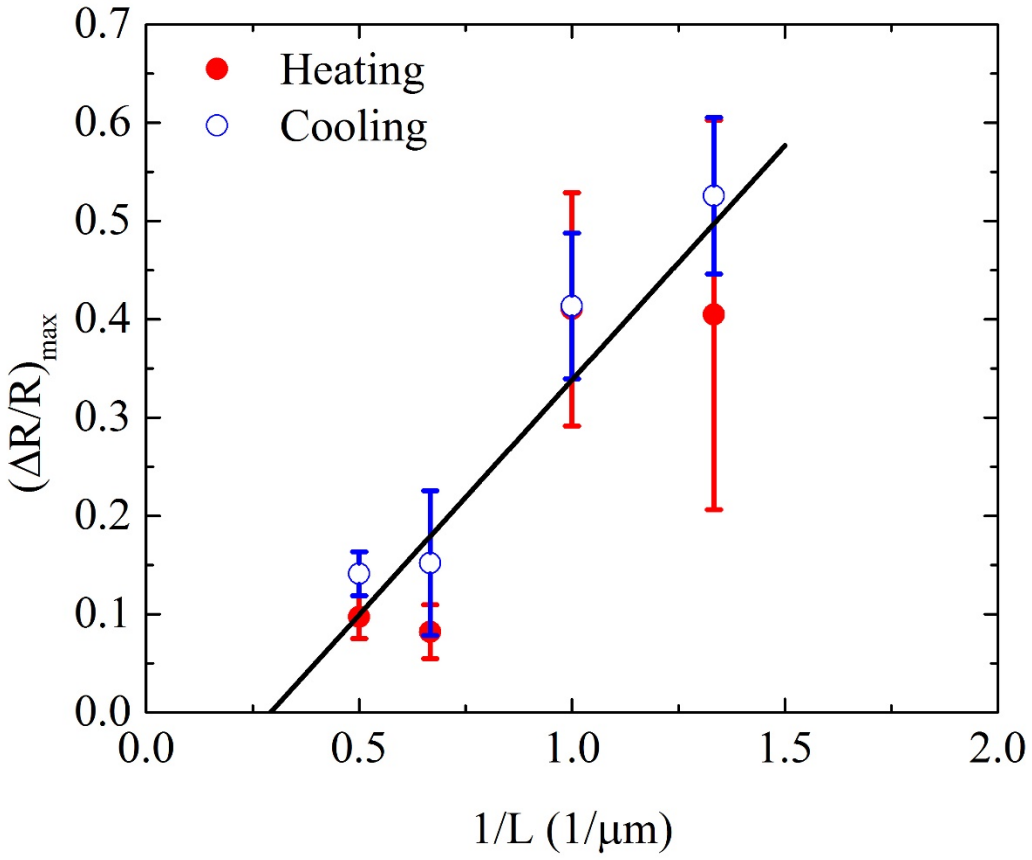

FIG. 2 (color online). Average value of the maximum jumps versus device length. The red solid (blue open) circles are the average maximum jumps from the heating (cooling) branches of the R-T measurements for each device. The error bars correspond the standard deviations of the maximum jumps. The black solid line is the linear fit of all the data points.

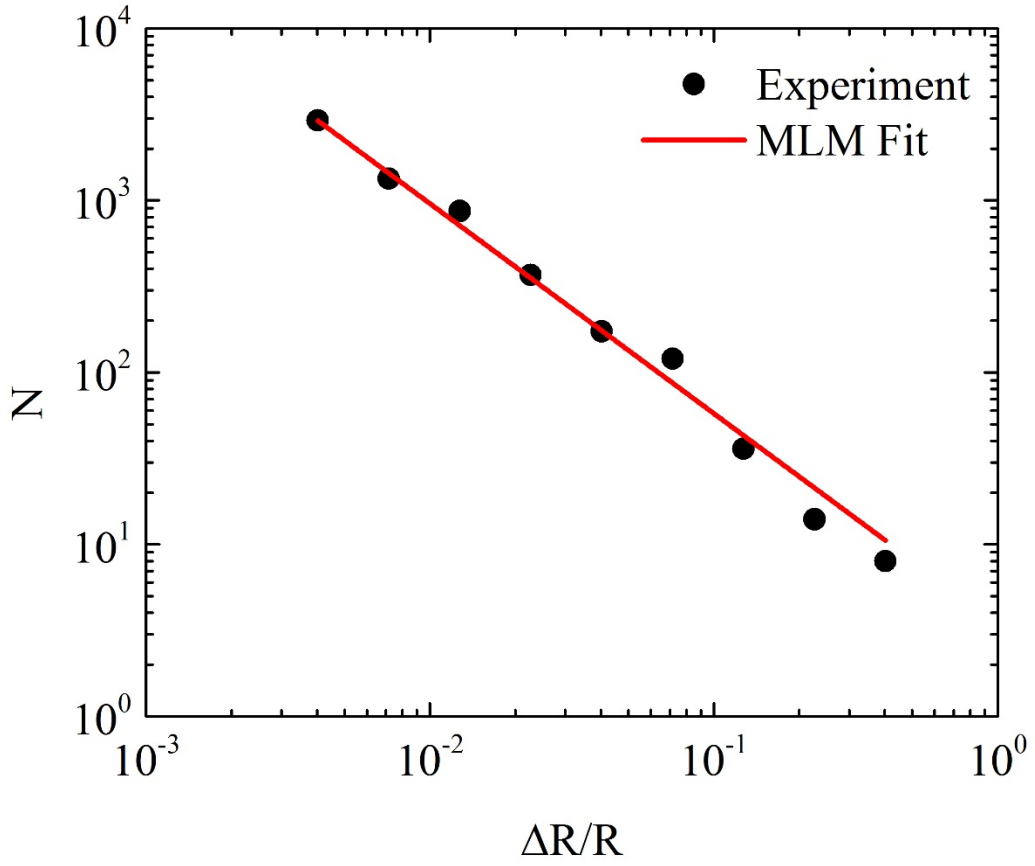

FIG. 3 (color online). The black solid circles show the histogram of different jump sizes plotted on a log-log scale from the heating branches of the R-T measurements for a 1 × 2 μm^2 device. The red solid line is a fit using the maximum likelihood method (MLM), showing a power law dependence. The exponent is $\alpha = 2.22 \pm 0.03$.

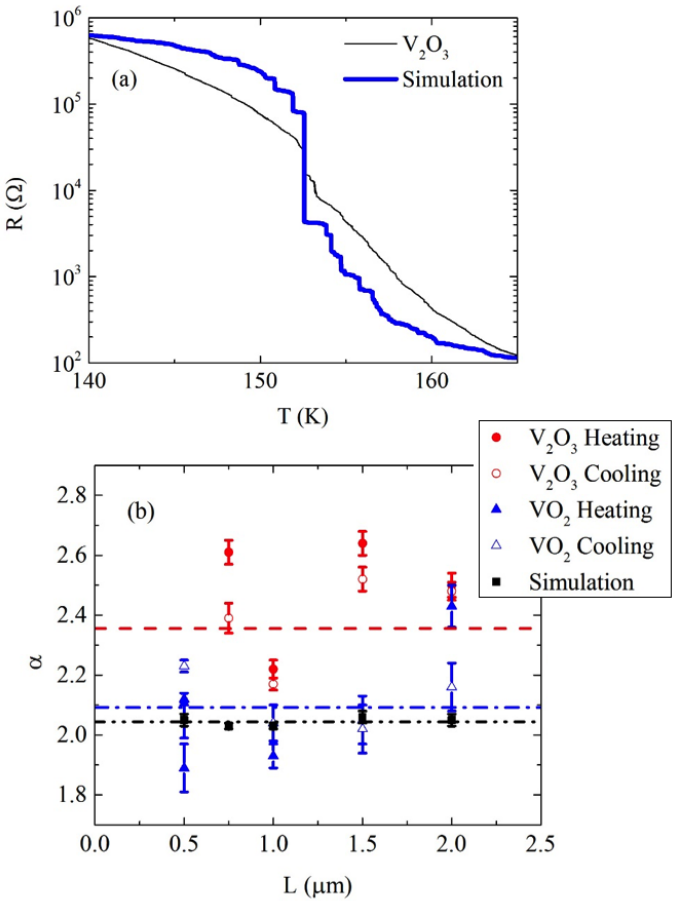

FIG. 4 (color online). (a) R-T of a 1 × 2 μm^2 device: simulation (thick blue solid line) and V_2O_3 (thin black solid line). (b) Comparison of the power law exponent of V_2O_3 (red circles), VO_2 (blue triangles) and the simulation (black squares). The solid (open) symbols are the exponents from the heating (cooling) branches of the R-T measurements. The error bars are the standard deviations given by — [26]. The dash lines indicate the average exponent of different devices for V_2O_3 (red dash line), VO_2 (blue dash dot line) and the simulation (black dash dot dot line).